HHS Public Access

Author manuscript

Neuroimage. Author manuscript; available in PMC 2021 January 05.

Published in final edited form as:

Neuroimage. 2021 January 01; 224: 117357. doi:10.1016/j.neuroimage.2020.117357.

Orientation-selective and directional deep brain stimulation in swine assessed by functional MRI at 3T

Julia P. Slopsema[a], **Antonietta Canna**[b], **Michelle Uchenik**[a], **Lauri J. Lehto**[b], **Jordan Krieg**[a], **Lucius Wilmerding**[a], **Dee M. Koski**[b], **Naoharu Kobayashi**[b], **Joan Dao**[a], **Madeline Blumenfeld**[a], **Pavel Filip**[b,e], **Hoon-Ki Min**[c], **Silvia Mangia**[b,#], **Matthew D. Johnson**[a,d,#], **Shalom Michaeli**[b,#,*]

[a]Department of Biomedical Engineering, University of Minnesota

[b]Department of Radiology, Center for Magnetic Resonance Research, University of Minnesota

[c]Department of Radiology, Mayo Clinic

[d]Institute for Translational Neuroscience, University of Minnesota

[e]Department of Neurology, Charles University, First Faculty of Medicine and General University Hospital, Prague, Czech Republic

Abstract

Functional MRI (fMRI) has become an important tool for probing network-level effects of deep brain stimulation (DBS). Previous DBS-fMRI studies have shown that electrical stimulation of the ventrolateral (VL) thalamus can modulate sensorimotor cortices in a frequency and amplitude dependent manner. Here, we investigated, using a swine animal model, how the direction and orientation of the electric field, induced by VL-thalamus DBS, affects activity in the sensorimotor cortex. Adult swine underwent implantation of a novel 16-electrode (4 rows × 4 columns) directional DBS lead in the VL thalamus. A within-subject design was used to compare fMRI responses for (1) directional stimulation consisting of monopolar stimulation in four radial directions around the DBS lead, and (2) orientation-selective stimulation where an electric field dipole was rotated 0°−360° around a quadrangle of electrodes. Functional responses were quantified in the premotor, primary motor, and somatosensory cortices. High frequency electrical stimulation through leads implanted in the VL thalamus induced directional tuning in cortical response patterns to varying degrees depending on DBS lead position. Orientation-selective stimulation showed maximal functional response when the electric field was oriented approximately parallel to the DBS lead, which is consistent with known axonal orientations of the cortico-thalamocortical pathway. These results demonstrate that directional and orientation-selective stimulation paradigms in the VL thalamus can tune network-level modulation patterns in the sensorimotor cortex, which may have translational utility in improving functional outcomes of DBS therapy.

[*]Corresponding author. shalom@cmrr.umn.edu (S. Michaeli).
[#]Joint senior authors

Supplementary materials

Supplementary material associated with this article can be found, in the online version, at doi:10.1016/j.neuroimage.2020.117357.

Keywords

Functional magnetic resonance imaging; High frequency stimulation; Thalamus; Motor cortex; Somatosensory cortex; Directional DBS; Orientation selective DBS

1. Introduction

The success of deep brain stimulation (DBS) therapy depends on the surgical precision of implanting a lead of electrodes to key nodal points within the brain (Papavassiliou et al., 2004; Richardson et al., 2009) and on the subsequent selection of stimulation settings to selectively modulate the pathways related to pathological activity (Hua et al., 1998; Kuncel et al., 2006). These spatial and functional targeting considerations are important in avoiding side effects induced by DBS, as well as in maintaining a wide therapeutic window between effective stimulation amplitudes and amplitudes that induce side effects. Recent advances in directional lead technology (Connolly et al., 2016; Contarino et al., 2014; Pollo et al., 2014; Steigerwald et al., 2016) and current steering (Butson and McIntyre, 2008; Martens et al., 2011; Barbe et al., 2014 Slopsema et al., 2018) have shown promise in enlarging therapeutic windows (Dembek et al., 2017; Reker et al., 2016) for improving clinical outcomes (Rebelo et al., 2018). However, little is known about the network-level changes in brain activity that occur when directing and steering electric fields through directional DBS leads.

Whole brain fMRI measurement of blood oxygenation level dependent (BOLD) contrast while electrically stimulating through a DBS lead implant (Carmichael et al., 2007; Gorny et al., 2013) has become a valuable tool to probe the mechanisms of DBS therapy at the network level. Porcine-model fMRI studies, for example, have shown how DBS targeting the ventral lateral (VL) thalamus (S.B. Paek et al., 2015), as well as the subthalamic nucleus, nucleus accumbens, globus pallidus, and centromedian-parafascicular nuclei can modulate network activity (Lee et al., 2011; Ross et al., 2016; Min et al., 2012; Kim et al., 2013). In particular, stimulation of the VL thalamus, which is the primary DBS target for treating Essential Tremor, can induce fMRI BOLD contrast in the sensorimotor cortex, basal ganglia, and cerebellum with contrast dependent on stimulation frequency and amplitude (S.B. Paek et al., 2015; Gibson et al., 2016).

The VL thalamus, or ventral intermediate nucleus (VIM) in humans, is well-suited to the use of directional DBS leads and current steering approaches given the clinical propensity to elicit side effects with stimulation (Rebelo et al., 2018; Lozano, 2000) for electrodes placed both within (Hubble et al., 1996; Benabid et al., 1991) and ventral-caudal to the nucleus (Sandvik et al., 2012; Hamel et al., 2007; Fytagoridis et al., 2013). This brain region consists of a convergence of axonal pathways that include cortico-thalamic/thalamo-cortical fibers and cerebello-thalamic fibers that are oriented approximately tangential to one another (Tracey et al., 1980; Asanuma et al., 1983; Pouratian et al., 2011). Improper surgical targeting can result in modulation of neighboring regions and pathways such as the corticospinal tract of internal capsule, leading to involuntary muscle contractions, and the medial lemniscus and somatosensory-receiving area of thalamus, leading to paresthesias.

Avoiding the spread of current into these regions and pathways is critical to limiting the likelihood of side effect inductions when programming DBS systems for Essential Tremor.

In this study, we have developed a network-level fMRI approach to measure the degree to which the pathways within and adjacent to a DBS target (VL thalamus) can be modulated using monopolar or bipolar stimulation delivered through a directional DBS lead. Previous computational studies have shown that one can enhance the selectivity of modulating pathways in the brain by increasing the segmentation of electrode contacts around and along the DBS lead (Teplitzky et al., 2016; Keane et al., 2012; Peña et al., 2017; Peña et al., 2018), using cathodic versus anodic stimulation (Anderson et al., 2019), and aligning the electric field to the direction of the axonal pathways of interest (Slopsema et al., 2018; Lehto et al., 2017). Here, we used fMRI in a porcine model to investigate the principles of controlling the primary direction of the electric field using a novel 16-channel DBS lead designed and built leveraging the same materials and manufacturing methods as used on commercially available clinical DBS leads, with the exception that the typical four rows of electrodes are each segmented into four radial contacts (Slopsema et al., 2019). While in the current study we implemented the hemodynamic response function (HRF) parameters used by Paek et al. (S.B. Paek et al., 2015) in similar experimental conditions to ours, we opted to additionally assess the functional responses by an independent component analysis (ICA) approach, which does not impose constraints on the HRFs.

2. Materials and methods

2.1. Research animals

Four female domestic swine (32.0 ± 2 kg) were used to investigate network-level effects of targeting the electric field direction and orientation around and along a novel 16 channel segmented DBS lead implanted in the VL thalamus. All procedures were approved by the University of Minnesota's Institutional Animal Care and Use Committee and abided by the United States Public Health Service (PHS) Policy on Humane Care and Use of Laboratory Animals.

2.2. Surgical procedure

Swine were sedated using a combination of Telazol (5 mg/kg i.m.) and xylazine (2 mg/kg i.m.), followed by atropine (0.04 mg/kg i.m.). Each swine was intubated, and anesthesia was maintained using isoflurane (1–3%). An MR-compatible swine head frame (Lee et al., 2011) was affixed to the swine followed by pre-operative anatomical imaging (Siemens 3T, software syngo MR VE11). Preoperative imaging included a 3D-MPRAGE (1 mm isotropic resolution, FOV 25.6 × 25.6 cm, number of slices = 176, TR/TE: 1900/2.93 ms, flip angle = 9°). These images were brought into Slicer (http://www.slicer.org) (Fedorov et al., 2012), registered with localization markers on the stereotactic frame using the SimpleStereotactic Slicer extension (J. Jacobs, UW Madison) (Edwards et al., 2018), and registered to a swine atlas (Félix et al., 1999; Saikali et al., 2010) using the Landmark Registration module (nonlinear, affine) in Slicer. An example is shown in Fig. 1a. The registration and stereotactic coordinate identification processes were conducted within a 15 min period between the conclusion of the pre-operative imaging and the beginning of the DBS implant

procedure. The SimpleStereotactic Slicer extension enabled input of: 1) a user-defined position of the DBS lead within the MR images and 2) a user-defined orientation of the DBS lead to avoid implanting the lead through the lateral ventricle or a cortical sulcus. The target was identified on the atlas as the VL thalamus on the border between the ventral anterior (VA) and ventral posterior (VP) regions of thalamus in the swine atlas (Fig. 1a).

In an aseptic procedure, a 14-mm cranial burr hole was created based on the position of a stylet through the calibrated Leksell head frame. The base of a Stimloc (Medtronic) burr hole cap was anchored to the cranium with two titanium bone screws. The dura was pierced to facilitate guiding an insertion cannula / stylet through the Leksell head frame and to 5-mm above the targeted implant depth. The stylet was then removed from the insertion cannula, and a novel 16-contact (4 rows × 4 columns) directional DBS lead (Fig. 1b) with similar form factor (diameter: 1.3 mm, 1.5 mm tall contacts, 0.5 mm spacing between rows) to clinically available human DBS leads (Slopsema et al., 2019) was implanted through the insertion cannula into the VL thalamus. The orientation of the DBS lead was controlled by a marker fiducial on one side of the DBS lead shank. The DBS lead was temporarily anchored to the Leksell head frame with a blunt set screw, the insertion cannula retracted, and the DBS lead secured to the burr hole ring using the Stimloc cap (Medtronic). The scalp was sutured closed to provide further support for the lead wires. The Leksell stereotactic frame was removed from the MR-compatible head frame before transporting the swine back to the 3T MRI scanner.

2.3. Imaging procedures

Post-surgery, the animal was returned to the 3T MRI Siemens Prisma system where the lead was connected to an Advanced Bionics Precision SC-1110 current-controlled pulse generator via Cat5 cables through a radio-frequency filter plate in the Faraday cage. Using the Advanced Bionics pulse generator, electrode impedances were measured in vivo through each segmented contact, which resulted in an average of 1630 ± 277 Ω across all electrodes and swine. The animal remained under isoflurane anesthesia (1–3%) throughout imaging and administered a bolus of pancuronium bromide (2 mg) followed by 3 mg/hr (i.v.) to reduce movements during the scans. Vitals including heart rate, $EtCO_2$, SpO_2, respiratory rate, and temperature were monitored throughout the procedure.

Anatomical scans were repeated for lead localization. These scans included an MPRAGE (parameters above) and an ultrashort echo time (UTE) (Bergin et al., 1991) scan (1.04 × 1.04 × 1.125 mm, FOV = 400 × 400 cm, slices = 144, flip angle = 5°, TR/TE: 2.6/0.11 ms, 640 Hz/pixel) that provided approximately a 50% reduction in susceptibility artifact (~ 3 mm) from the lead as compared to the MPRAGE artifact (~6 mm). A pre-implant MPRAGE was overlaid with a post-implant UTE (Fig. 1c) to identify the location of the implanted lead. Following anatomical scans, fMRI scans were performed using gradient-echo EPI (2.2 mm isotropic, FOV = 22 × 22 cm, slices = 34, flip angle = 90°, TR/TE: 2000/30 ms). To estimate which rows of contacts would provide the strongest response of the motor cortex, initial functional scans were completed in each swine using quads of 4 electrodes (2 rows × 2 columns) pointing in the medial direction with 3 mA of current per contact, BOLD contrast in the motor cortex, resulting from stimulation through two-row quads on the medial side of

the lead, was qualitatively compared using the Siemens (VE11C) on-line BOLD reconstruction. The quad of electrodes with the strongest BOLD contrast was identified, and the two rows defined by the quad were used for the directional stimulation and for the orientation-selective stimulation experiments.

2.4. Stimulation paradigms

Blood Oxygenation Level Dependent (BOLD) Contrast.—fMRI scans were performed over a 20 s baseline period (no stimulation), followed by 20 s of stimulation, and then a 60 s wash-out period (no stimulation), repeated three times for a total of ~5 min for each trial. All stimulation paradigms used a 130 Hz pulse train with an initial phase pulse width of 90 μs delivered through the Advanced Bionics pulse generator.

Directional Stimulation.—Using the two adjacent rows identified to have the highest response in motor cortex during the baseline qualitative scans were then used in the directional stimulation experiments. Directional stimulation was applied simultaneously through two contacts along a single column and with 6 mA of current through each contact. Stimulation was applied through these columnar contact pairs in each of the four radial directions around the lead (Fig. 2a) using the same stimulation paradigm and EPI sequence as described above. The current used in this study was higher than what is typically used clinically, which was necessary to achieve robust stimulation-induced BOLD signaling in the presence of presumed edema around the acutely implanted DBS lead (Moffitt and McIntyre, 2005) and anesthetized conditions.

Orientation-Selective Stimulation.—Within the previously optimized quad of electrodes, stimulation settings were applied using a cathode-anode dipole rotated relative to the center of the quad in 8 directions (Fig. 2b). Stimulation was applied at 6 mA, which was half of the current applied in the directional stimulation protocol. This reduction was due to the amount of current applied through a single electrode as the number of active contacts varied with the stimulation direction. Specifically, when the electric field was oriented at 45°/135°/225°/315° with respect to the lead only two contacts are active in a bipolar configuration (±6 mA, bipolar). For the electric field orientations at 0°/90°/180°/270°, the bipolar configuration was split across 4 contacts, therefore ±3 mA of current was applied through each contact for a total of 6 mA (bipolar).

2.5. Statistical analysis

Preprocessing of functional data: general linear model analysis.—Image data preprocessing and general linear model (GLM) analysis were performed in BrainVoyager 21.4 (Brain Innovation, Maastricht, The Netherlands, www.brainvoyager.com). Preprocessing of functional time series were performed separately for each paradigm and animal. From the 150 volumes collected for each trial, the first 20 volumes were removed to guarantee full signal stabilization. Preprocessing included: slice scan time correction using a cubic spline interpolation procedure; head motion correction by a rigid re-alignment of all the volumes to the first volume based on a Levenberg-Marquardt algorithm, optimizing three translation and three rotation parameters on a resampled version of each image; spatial smoothing with an isotropic gaussian kernel of 4.4 mm FWHM, temporal filtering using a

high-pass filter with cut-off set to 0.008 Hz to reduce linear and non-linear trends in the time-courses; alignment of the functional time-series to the anatomical T1w reference acquired after implantation. In order to extract the functional maps, a single study GLM was first applied at a voxel-based level. The predictor was defined as a box-car representing the stimulation paradigm convolved with a double-gamma HRF as used previously (Paek et al., 2015) (onset −6, response undershoot ratio 3, time to response peak 15 s and time to undershoot peak 25 s). The six motion parameters were added in the GLM model as confound predictors. A correction for serial correlation was applied using fit-refit procedure with a second-order autoregressive model applied to the GLM residuals. Z-transformation was applied to the time courses before the GLM fitting.

A swine atlas (Félix et al., 1999) was registered to the post-op MPRAGE. This atlas was used to segment out the motor, premotor, and somatosensory cortices as regions of interest (Fig. 3a). A false discovery rate (FDR) threshold of $p<0.001$ was applied to the t-statistic maps to quantify the mean effect in each region of interest (Fig. 3b). As an example, the mean time series of the voxels for each cortex was normalized relative to the last 10 s of the baseline prior to the first block of stimulation as shown in Fig. 3c. Results of the GLM fitting were also reported at a region of interest (ROI) level in correspondence of the 3 primary regions of premotor, primary motor and somatosensory cortices (Supplementary Figure 1). For comparison of average t-statistic in the sensorimotor cortices, Friedman tests were performed for the directional and orientation-selective results.

Preprocessing of functional data: independent component analysis (ICA).—In order to analyze the data without a-priori assumptions on the shape of the HRF, we additionally performed an independent component analysis (ICA) of each time-series (LeVan and Gotman, 2009; Moeller et al., 1987). In this case, the full functional time-series were first preprocessed with SPM12 (www.fil.ion.ucl.ac.uk/spm/) running on MATLAB R2016a. Pre-processing steps were similar to the GLM analysis described above, and included slice-time correction, head motion correction and smoothing with an isotropic Gaussian kernel of 4.4 mm FWHM, alignment to the anatomical reference. To compute the ICA, we used the MELODIC v.3.15 toolbox of FSL v.6.0.1 (https://fsl.fmrib.ox.ac.uk/fsl/) with free dimensionality, i.e., letting MELODIC establish the number of components that explain the variance of the data. For each paradigm (total of 48 experimental sessions), a visual inspection of the independent component time-series was performed to identify the components that unambiguously correlated with the stimulation paradigm (Supplementary Figure 2). For 46 out of 48 experimental sessions, we identified either one or no components. However, for 2 directional paradigms of one animal, two independent components were found to correlate with the stimulation paradigm. For these specific cases, we reduced the dimensionality of the ICA to achieve only one component correlating with the stimulation paradigm. The corresponding spatial maps of the ICA were then shown as z-statistic maps with values between 2.5 and 5, and the mean z-statistic of the final ICA maps were calculated for each region of interest. Friedman tests were again performed to compare the z-statistic in the sensorimotor cortices for the directional and orientation-selective results.

The data and code supporting the findings of this study are available from the corresponding author, upon reasonable request. The data and code sharing comply with requirements of the funding bodies and institutional practices.

3. Results

3.1. Sensorimotor fMRI bold contrast induced by VL-thalamus DBS

Directional DBS leads were implanted in the VL thalamus (Fig. 4) in four swine. Functional responses of the motor, premotor, and somatosensory cortices were quantified using fMRI while stimulating through the directional DBS lead. Two stimulation paradigms were investigated: directional stimulation around the DBS lead and orientation-selective stimulation around a quad of electrodes on the DBS lead. Atlas-based segmentation of the sensorimotor cortex was used for the analysis of the functional maps. In both cases, mostly negative BOLD responses were detected. The quality of the GLM fitting was generally good for 3 swine, but was suboptimal for one swine (namely swine 2), in which case the shape of the functional responses were not fully captured by the used HRF (Supplementary Figure 1).

3.2. Directional stimulation

Directional stimulation was investigated using two row-adjacent cathodes in each of the 4 columns on the DBS lead (Fig 2a). While significant BOLD contrast was present in the motor, premotor, and somatosensory cortices in all four animals (Fig. 5a), the degree to which these responses depended on the direction of the cathode pair in turn depended on the implant location (Fig. 5b,c). In swine 1 and 3, the BOLD contrast in all three cortical regions did not depend on the direction of the active electrode pair. Swine 2 exhibited the most significant directional tuning, with the strongest response of all three cortices in the medial posterior, lateral posterior, and lateral anterior directions, and reduced response in the lateral anterior direction. Swine 4 exhibited mixed results with little directional tuning in the motor and premotor cortices and modest directional tuning in the motor cortex such that the medial posterior direction provided greatest response in terms of the GLM. With a more refined ICA analysis, Swine 4 showed no response in the medial anterior direction and low response in the other three directions. Comparing directions using a Friedman test, the functional response in all three cortices was not significantly related to the direction of stimulation using the GLM method (motor: $p = 0.68$; premotor: $p = 0.96$; somatosensory: $p = 0.44$), or the ICA method (motor: $p = 0.53$; premotor: $p = 0.80$; somatosensory: $p = 0.90$).

3.3. Orientation-Selective stimulation

Orientation-selective stimulation was applied by rotating the primary direction of the electric field around a quad of electrodes positioned on the medial side of the directional DBS lead in 45° increments with 0°/180° (superior/inferior) representing electric fields parallel to the lead and 90°/270° (posterior/anterior) representing electric fields perpendicular to the lead using GLM analysis (Fig. 6a) and ICA (Fig. 6b). Orientation-selective tuning of the BOLD signal was observed in all four swine with GLM analysis, and three out of four swine using the ICA method. Comparing directions using a Friedman test and the GLM analysis, the functional response in the premotor cortex was significantly related to orientation of stimulation in the premotor cortex ($p = 0.01$) but was not significant in the motor ($p = 0.73$)

and somatosensory cortices ($p = 0.19$). A trend of orientation selectivity was observed in the premotor cortex also when using the z-scores from the ICA approach ($p = 0.09$), but not in the motor ($p = 0.25$) or somatosensory ($p = 0.14$) cortex.

Orientation-selective stimulation resulted in a differential effect on cortical regions in each swine. DBS in Swine 1, the GLM revealed maximum response at 90°, 180°, and 180° for the motor, premotor and somatosensory cortices, respectively, while ICA analysis identified response at 0°/180° in all three cortices. Swine 2 showed largely equivalent response across cortical regions of interest using the GLM and ICA with the exception of a peak at 270° in the premotor cortex using ICA. Swine 3 exhibited modest tuning in the motor and premotor cortices using the GLM with peaks at 360° and 180° respectively and little tuning in the somatosensory cortex, no independent components were related to the stimulation using ICA. Swine 4 showed orientation-selective turning in all three cortices with maximums at 315°, 0°/360°, and 0°/360° for the motor, premotor and somatosensory cortices respectively using the GLM method and 0°/360° in all three cortices using ICA.

4. Discussion

In this study, we showed how directional and orientation-selective stimulation through a directional DBS lead can differentially modulate activity patterns in the primary motor, premotor, and somatosensory cortices. While directional stimulation has become a promising approach to improve clinical outcomes of DBS therapy (Dembek et al., 2017; Rebelo et al., 2018), the utilization of orientation-selective stimulation concepts have yet to be broadly leveraged in the clinical context.

4.1. Neural pathways involved in the effects of vl thalamus dbs

Our results demonstrated that high-frequency electrical stimulation of the VL thalamus resulted in functional response of the primary, premotor, and somatosensory cortices. These results are consistent with previous fMRI studies of the VL thalamus, which showed modulation of the primary motor cortex, premotor cortex, and somatosensory cortex in a frequency and amplitude dependent manner in a swine model (S.B. Paek et al., 2015). Additionally, positron emission tomography studies have shown increases in regional cerebral blood flow in the motor cortex during stimulation of the VL thalamus (Ceballos-Baumann et al., 2001; Haslinger et al., 2003). The functional response in the sensorimotor cortex could be attributed to several pathways and mechanisms. Tracing of the cerebello-thalamo-cortical circuit (Asanuma et al., 1983; Ilinsky and Kultas-Ilinsky, 1987; Mason et al., 1996; Lee et al., 2019) have shown that the VL region is reciprocally connected with the motor cortex (Ilinsky and Kultas-Ilinsky, 2002). Given these connections, DBS of the VL thalamus is likely to excite thalamo-cortical fibers resulting in orthodromic response of the motor cortices and excite cortico-thalamic fibers resulting in antidromic response of the motor cortex (Kultas-Ilinsky et al., 2003; Guillery, 1995; Kakei et al., 2001). A previous magnetoencephalography study supports the notion that such response of sensorimotor cortex could be due to antidromic stimulation of corticofugal pathways in addition to orthodromic response of the motor cortex (Hartmann et al., 2018). It is worth noting that the most prominent cortical region modulated by VL thalamus DBS in our study was the

premotor cortex across the four animals and the degree to which this occurred could be tuned through directional DBS. Stimulation paradigms consistently induced negative BOLD contrast in the sensorimotor cortex, as assessed using the GLM method. This is consistent with previous studies based on the amplitude and frequency used in this work (Gibson et al., 2016).

4.2. Location-dependent directional tuning

Studies have shown that directional DBS can reduce thresholds for therapy and increase thresholds for side effects when implanted in the subthalamic nucleus for treatment of Parkinson's disease (Contarino et al., 2014; Pollo et al., 2014; Steigerwald et al., 2016; Dembek et al., 2017; Reker et al., 2016) and when implanted in the VIM thalamus for treatment of Essential Tremor (Pollo et al., 2014; Rebelo et al., 2018). In the present study, directional stimulation was applied through two contacts in a single column in 4 radial directions around the lead targeting the homologue of Vim thalamus. ICA analysis in Swine 1 and 2 showed greater response of the premotor cortex (Fig. 5b) compared to the motor and somatosensory cortices. This is likely due to the DBS lead implant having been located slightly anterior of the VL/VP border. Tracing studies have shown that the anterior region of VL has proportionally greater connections to premotor cortex, whereas the posterior region of VL has proportionally greater connections to the primary motor cortex (Fang et al., 2006). In addition, activity in the motor cortex when stimulation was directed lateral could be related to current spreading into the internal capsule. Thus, stimulation directed to either the medial or lateral side of the lead could result in response of the motor cortex through different anatomical pathways. In contrast, swine 3 and 4 were implanted closer to the border between the VL and VP nuclei, and response was more equally distributed across the three cortices (Fig. 5a).

The direction of stimulation resulted in approximately equal response of the different cortices in swine 1 and 3; however, response in swine 2 was weakest in the lateral anterior direction, and in swine 4 maximum and minimum response was dependent on the cortical region analyzed. ICA analysis in Swine 3 did not identify any components related to the stimulus as can be seen in Supplementary Figure 2. Overall this swine had a much noisier fMRI signal which could be attributed to motion. In general, there were no strong differences in cortical modulation as the active electrodes were directed around the lead; this reduced effect of directional stimulation relative to stronger effects shown in the literature (Rebelo et al., 2018) could be a result of shunting of the current along and around the lead due to formation of edema immediately after lead implantation (Vedam-Mai et al., 2011). We would expect this directional effect to be more pronounced for a chronically implanted DBS lead in which edema events have resolved (Vedam-Mai et al., 2011). In support of this argument, a previous study by Dembek et al., showed no functional outcome differences between ring-mode stimulation (i.e. grouping all contacts around a segmented lead) and directional stimulation in a short-term cross over; however, they did show an improvement in therapeutic windows using directional contacts compared to circular stimulation at three and six month follow-ups (Dembek et al., 2017). The amplitude of stimulation also can have a large effect on whether or not directional stimulation can be achieved. For instance, computational models have predicted that when stimulation amplitudes are too small, there

is no activation of axons in any direction, while stimulation with too high of an intensity can activate axons in multiple directions especially if edema is present around the implant (Slopsema et al., 2018; Lehto et al., 2017).

4.3. Orientation-selective stimulation provided tuned modulation with less current

Current steering based on the orientation of the electric field is a relatively new concept in DBS given the advent of directional DBS lead technology. The approach has shown to be valuable in computational and small animal studies (Slopsema et al., 2018; Lehto et al., 2017). Here, using a clinically-viable directional DBS lead design, we showed in a large animal that the functional response of the motor, premotor, and somatosensory cortices by VL thalamus DBS could be modulated based on orientation of the electric field. Stimulation at 0° and 180° would be expected to induce equal response in homogeneous tissue (Slopsema et al., 2018). However, since the tissue in the nuclei is inhomogeneous and anisotropic, there are two competing effects, the primary direction of the electric field relative to the orientation of adjacent fibers as well as the proximity of the cathode to the target due a non-symmetric distribution of current using bipolar and monopolar configurations (Schmidt and van Rienen, 2012; McIntyre et al., 2004; Chaturvedi et al., 2013). An orientation-selective approach to stimulation is potentially advantageous as the current can be more precisely steered toward the region or pathway of interest while limiting the spread of current to neighboring regions via a bipolar or multipolar configuration (Chaturvedi et al., 2013).

One key point to interpreting the results is appreciating the unequal distance between the anode and cathode contacts for each electric field orientation. When the field was oriented parallel to the lead, the edge-to-edge distance between anodes and cathodes was 500 μm, whereas when the field was oriented perpendicular to the lead, the edge-to-edge distance between anodes and cathodes was 180 μm. This could result in a shorting effect between the anode and cathode. However, if this were the case, the diagonal off-axis configurations (i.e. 45°, 135°, 225°, 315°), which had a proximal corner-to-corner distance of 531 μm, did not show a stronger effect in most cases (Fig. 6). Indeed, the 0° or 180° orientation was most prominent in all eight of the twelve cortex measurement using GLM and were the only angles showing any response using ICA analysis in two swine.

4.4. Value of 4 × 4 lead

This study demonstrates the utility of a novel directional DBS lead for preclinical use with four rows and four contacts within each row (Slopsema et al., 2019), which provides flexibility to steer current along and around a DBS lead. Computational studies have shown that directional leads with more than four radial electrodes result in minimal improvement in the ability to steer current around a lead (Teplitzky et al., 2016). Current clinical leads provide three contacts around the lead and only have segments in the middle two rows. Clinical studies have used bipolar configurations axially around the lead to reduce side effects and improve therapy in a single patient study (Reker et al., 2016). The design provided additional flexibility to steer current axially around the lead and along the lead in the experiments, and here we demonstrated that segmented contacts in multiple rows can be

used with bipolar configurations to further steer current using orientation-selective paradigms.

4.5. Study limitations

DBS implants targeted the VL region of the thalamus as it is a homologue of the clinically relevant target of DBS for human Essential Tremor. Though the implants targeted the same region, there was variability of implantation across swine as shown in Fig. 4. This implant variability is likely due to the accuracy with which we were able to register an atlas to the imaging data, the precision of our stereotactic frame, and brain shift following the craniectomy. We attempted to mitigate these errors through training on atlas registration, maximizing precision with the frame and equipment, and implanting the lead within five minutes of the craniectomy.

Of note, although the pig brain is closer in volume and structure to the human brain than the rodent brain, there are marked differences between pigs and humans in the volume of brain size (human: 1300–1400 g, rhesus monkey: 90–97 g, domestic swine: 180 g, rodent: 2 g) (Springer, 2011; Hofman, 1985). Due to the smaller size of the pig brain while using a human probe, the current field might be too large to see more fine steering discrimination. For example, stimulation of the VL shown here often lead to BOLD contrast in the somatosensory cortex, likely due to current spread to the medial lemniscus associated with paresthesias (Gibson et al., 2016). In a larger human brain, the direction of stimulation may be more precisely tuned to individual pathways. Previous studies have seen a stimulation amplitude effect, higher voltage stimulation causing less regional specificity in cortical BOLD response in a thalamic DBS swine study (Kim et al., 2013). For the acute animal experimental paradigm tested, each stimulus setting could only be tested with a single trial and three repetitions within each trial; future studies may benefit from animal preparations that are chronic leveraging periodic fMRI tests over multiple days in the same animal.

Finally, the negative BOLD responses observed in our studies were similar to those observed previously in the anaesthetized swine (S.B. Paek et al., 2015). However, we also noticed that the GLM fitting was suboptimal in one out of 4 animals (Supplementary Figure 1), highlighting that the use of a single HRF, although modified to account for differences with the canonical HRF used for awake humans, did not fully capture the variability of responses observed in our dataset. Some level of caution is thus warranted when evaluating the results of a GLM approach with a fixed HRF, and it is advisable to display the GLM fitting results at least at an ROI-based level to verify whether there are different shapes of the functional responses that deserve special consideration. Notably, the definition of the most proper and flexible HRF for the anaesthetized swine during DBS merits systematic investigations that go beyond the scope of the current study. On the other hand, we opted to tackle the issue of different shapes of functional responses by additionally evaluating the study outcomes with ICA, i.e., with an approach inherently free from assumptions on the HRF. The ICA approach qualitatively reproduced the main findings of the present study observed with GLM analysis. Besides inter-subject differences in the shape of the IC, directional paradigms almost always exhibited a stimulus-related IC, whereas stimulus-related ICs were observed only for a

subset of OSS paradigms, typically at 0° or 180° Such observations support a higher degree of selectivity achievable with OSS vs directional paradigms.

5. Conclusions

Here we investigated the use of a novel 16-contact directional DBS lead to steer current axially in a monopolar manner and to steer the primary direction of an electric field around a quad of electrode contacts. Directional stimulation axially around the lead provided differential response in some sensorimotor cortices. We additionally presented in vivo evidence that steering the primary orientation of the electric field can be used to maximize cortical response when the field is approximately aligned with an adjacent pathway. While the swine model does not provide an exact homologue to the VIM thalamus in humans, the paradigms presented here show promise for translation to more selectively activate pathways of interest in future clinical studies.

Supplementary Material

Refer to Web version on PubMed Central for supplementary material.

Acknowledgements

This work was supported by the National Institutes of Health (R01-NS081118, R01-NS094206, P50-NS098573, U01-NS103569), NSF-GRFP (00039202, JPS), and the EU H2020 Marie Sk ł odowska RISE project (#691110, MICROBRADAM). We thank the Center for Magnetic Resonance Research (NIH core grants: P41-EB015894, P30-NS076408, U54-MH091657) and University of Minnesota Foundation for help with the MRI imaging used in this study (Dee Koski, Erik Solheid). We thank Heraeus Medical Components for the DBS lead (Robert Cass, Mark Hjelle, Mitch Lark, Paul Noffke, David Ohmann), NRTL lab members (Lauren Madden, Annie Brinda, Mojgan Goftari), and the Mayo Clinic Neuroengineering Group for guidance and fabrication of the stereotactic frame and targeting software (Dr. Kendall Lee, Steven Goerss, Dr. Joshua Jacobs).

Abbreviation:

DBS	deep brain stimulation
VIM	ventral intermediate nucleus of thalamus
VL	ventrolateral nucleus of thalamus
VP	ventral posterior nucleus of thalamus
VA	ventral anterior nucleus of thalamus
fMRI	functional Magnetic Resonance Imaging
BOLD	blood-oxygen level dependent

References

Anderson DN, Duffley G, Vorwerk J, Dorval AD, Butson CR, 2019 Anodic stimulation misunderstood: preferential activation of fiber orientations with anodic waveforms in deep brain stimulation. J Neural Eng 16 (1), 016026. doi: 10.1088/1741-2552/aae590. [PubMed: 30275348]

Asanuma C, Thach T, Jones EG, 1983 Distribution of cerebellar terminations in the ventral lateral thalamic region of the monkey. Brain ResRev 5, 237–265.

Barbe MT, Maarouf M, Alesch F, Timmermann L, 2014 Multiple source current steering–a novel deep brain stimulation concept for customized programming in a Parkinson's disease patient. Parkinsonism Relat. Disord 20 (4), 471–473. doi: 10.1016/j.parkreldis.2013.07.021. [PubMed: 24041939]

Benabid AL, Pollak P, Hoffmann D, et al., 1991 Long-term suppression of tremor by chronic stimulation of the ventral intermediate thalamic nucleus. The Lancet 337 (8738), 403–406. doi: 10.1016/0140-6736(91)91175-T.

Bergin CJ, Pauly JM, Macovski A, 1991 Lung Parenchyma: projection Reconstruction MR Imaging. Radiology 777–781 Published online. [PubMed: 2027991]

Butson CR, McIntyre CC, 2008 Current steering to control the volume of tissue activated during deep brain stimulation. Brain Stimul 1 (1), 7–15. doi: 10.1016/j.brs.2007.08.004. [PubMed: 19142235]

Carmichael DW, Pinto S, Limousin-Dowsey P, et al., 2007 Functional MRI with active, fully implanted, deep brain stimulation systems: safety and experimental confounds. Neuroimage 37 (2), 508–517. doi: 10.1016/j.neuroimage.2007.04.058. [PubMed: 17590355]

Ceballos-Baumann AO, Boecker H, Fogel W, et al., 2001 Thalamic stimulation for essential tremor activates motor and deactivates vestibular cortex. Neurology 56 (10), 1347–1354. [PubMed: 11376186]

Chaturvedi A, Luján JL, McIntyre CC, 2013 Artificial neural network based characterization of the volume of tissue activated during deep brain stimulation. J Neural Eng 10 (5), 056023. doi: 10.1088/1741-2560/10/5/056023. [PubMed: 24060691]

Connolly AT, Vetter RJ, Hetke JF, et al., 2016 A Novel Lead Design for Modulation and Sensing of Deep Brain Structures. IEEE Transactions on Biomedical Engineering 63 (1), 148–157. doi: 10.1109/TBME.2015.2492921. [PubMed: 26529747]

Contarino MF, Bour LJ, Verhagen R, et al., 2014 Directional steering: a novel approach to deep brain stimulation. Neurology 83 (13), 1163–1169. doi: 10.1212/WNL.0000000000000823. [PubMed: 25150285]

Dembek TA, Reker P, Visser-Vandewalle V, et al., 2017 Directional DBS increases side-effect thresholds-A prospective, double-blind trial: directional Dbs Increases Side-Effect Thresholds. Movement Disorders 32 (10), 1380–1388. doi: 10.1002/mds.27093. [PubMed: 28843009]

Edwards CA, Rusheen AE, Oh Y, et al., 2018 A novel re-attachable stereotactic frame for MRI-guided neuronavigation and its validation in a large animal and human cadaver model. J Neural Eng 15 (6), 066003. doi: 10.1088/1741-2552/aadb49. [PubMed: 30124202]

Fang P−C, Stepniewska I, Kaas JH, 2006 The thalamic connections of motor, premotor, and prefrontal areas of cortex in a prosimian primate (Otolemur garnetti). Neuroscience 143 (4), 987–1020. doi: 10.1016/j.neuroscience.2006.08.053. [PubMed: 17055664]

Fedorov A, Beichel R, Kalpathy-Cramer J, et al., 2012 3D Slicer as an image computing platform for the Quantitative Imaging Network. Magn Reson Imaging 30 (9), 1323–1341. doi: 10.1016/j.mri.2012.05.001. [PubMed: 22770690]

Félix B, Léger M−E, Albe-Fessard D, et al., 1999 Stereotaxic atlas of the pig brain. Brain Res. Bull 49 (1), 1–137. [PubMed: 10466025]

Fytagoridis A, Sjöberg R, Åström M, Fredricks A, 2013 Effects of deep brain stimulation in the caudal Zona incerta on verbal fluency. S Karger 91 (1), 24–29. doi: 10.1159/000342497.

Gibson WS, Jo HJ, Testini P, et al., 2016 Functional correlates of the therapeutic and adverse effects evoked by thalamic stimulation for essential tremor. Brain 139 (8), 2198–2210. doi: 10.1093/brain/aww145. [PubMed: 27329768]

Gorny KR, Presti MF, Goerss SJ, et al., 2013 Measurements of RF heating during 3.0-T MRI of a pig implanted with deep brain stimulator. Magn Reson Imaging 31 (5), 783–788. doi: 10.1016/j.mri.2012.11.005. [PubMed: 23228310]

Guillery RW, 1995 Anatomical evidence concerning the role of the thalamus in corticocortical communication: a brief review. Journal of Anantomy 187, 583–592.

Hamel W, Herzog J, Kopper F, et al., 2007 Deep brain stimulation in the subthalamic area is more effective than nucleus ventralis intermedius stimulation for bilateral intention tremor. Acta Neurochir (Wien) 149 (8), 749–758. doi: 10.1007/s00701-007-1230-1. [PubMed: 17660940]

Hartmann CJ, Hirschmann J, Vesper J, Wojtecki L, Butz M, Schnitzler A, 2018 Distinct cortical responses evoked by electrical stimulation of the thalamic ventral intermediate nucleus and of the subthalamic nucleus. NeuroImage: Clinical 20, 1246–1254. doi: 10.1016/j.nicl.2018.11.001. [PubMed: 30420259]

Haslinger B, Boecker H, Büchel C, et al., 2003 Differential modulation of subcortical target and cortex during deep brain stimulation. Neuroimage 18 (2), 517–524. doi: 10.1016/S1053-8119(02)00043-5. [PubMed: 12595204]

Hofman MA.., 1985 Size and Shape of the Cerebral Cortex in Mammals. I. The Cortical Surface. Brain, Behavior & Evolution 27, 28–34.

Hua SE, Lenz FA, Zirh TA, Reich SG, Dougherty PM, 1998 Thalamic neuronal activity correlated with essential tremor. Journal of Neurology, Neurosurgery & Psychiatry 64 (2), 273–276.

Hubble J, Busenbark K, Wilkinson S, Penn R, Lyons K, Koller W, 1996 Deep brain stimulation for essential tremor. Neurology 46, 1150–1153. [PubMed: 8780109]

Ilinsky I, Kultas-Ilinsky K, 1987 Sagittal cytoarchitectonic maps of the macaca mulatta thalamus with a revised nomenclature of the motor-related nuclei validated by observations on their connectivity. JCompNeurol 262, 331–364.

Ilinsky IA, Kultas-Ilinsky K, 2002 Motor thalamic circuits in primates with emphasis on the area targeted in treatment of movement disorders. Movement Disorders 17 (S3), S9–S14. doi: 10.1002/mds.10137. [PubMed: 11948750]

Kakei S, Na J, Shinoda Y, 2001 Thalamic terminal morphology and distribution of single corticothalamic axons originating from layers 5 and 6 of the cat motor cortex. J. Comp. Neurol 437 (2), 170–185. doi: 10.1002/cne.1277. [PubMed: 11494250]

Keane M, Deyo S, Abosch A, Bajwa JA, Johnson MD, 2012 Improved spatial targeting with directionally segmented deep brain stimulation leads for treating essential tremor. J Neural Eng 9 (4), 046005. doi: 10.1088/1741-2560/9/4/046005. [PubMed: 22732947]

Kim JP, Min H−K, Knight EJ, et al., 2013 Centromedian-Parafascicular Deep Brain Stimulation Induces Differential Functional Inhibition of the Motor, Associative, and Limbic Circuits in Large Animals. Biol. Psychiatry 74 (12), 917–926. doi: 10.1016/j.biopsych.2013.06.024. [PubMed: 23993641]

Kultas-Ilinsky K, Sivan-Loukianova E, Ilinsky IA, 2003 Reevaluation of the primary motor cortex connections with the thalamus in primates. J. Comp. Neurol 457 (2), 133–158. doi: 10.1002/cne.10539. [PubMed: 12541315]

Kuncel AM, Cooper SE, Wolgamuth BR, et al., 2006 Clinical response to varying the stimulus parameters in deep brain stimulation for essential tremor. Movement Disorders 21 (11), 1920–1928. doi: 10.1002/mds.21087. [PubMed: 16972236]

Lee J, Jo HJ, Kim I, et al., 2019 Mapping BOLD activation by pharmacologically evoked tremor in swine. Front Neurosci 13, 985. [PubMed: 31619955]

Lee KH, Chang S-Y, Jang D-P, et al., 2011 Emerging techniques for elucidating mechanism of action of deep brain stimulation. In: 2011 Annual International Conference of the IEEE Engineering in Medicine and Biology Society. IEEE, pp. 677–680. doi: 10.1109/IEMBS.2011.6090152.

Lehto LJ, Slopsema JP, Johnson MD, et al., 2017 Orientation selective deep brain stimulation. J Neural Eng 14 (1), 016016. doi: 10.1088/1741-2552/aa5238. [PubMed: 28068296]

LeVan P, Gotman J, 2009 Independent component analysis as a model-free approach for the detection of BOLD changes related to epileptic spikes: a simulation study. Hum Brain Mapp 30 (7), 2021–2031. doi: 10.1002/hbm.20647. [PubMed: 18726909]

Lozano AM, 2000 Vim thalamic stimulation for tremor. Arch. Med. Res 31 (3), 266–269. [PubMed: 11036177]

Martens HC, Toader E, Decre MM, et al., 2011 Spatial steering of deep brain stimulation volumes using a novel lead design. Clinical neurophysiology : official journal of the International Federation of Clinical Neurophysiology 122 (3), 558–566. doi: 10.1016/j.clinph.2010.07.026. [PubMed: 20729143]

Mason A, Ilinsky IA, Beck S, Kultas-Ilinsky K, 1996 Reevaluation of synaptic relationships of cerebellar terminals in the ventral lateral nucleus of the rhesus monkey thalamus based on serial

section analysis and three-dimensional reconstruction. Exp Brain Res 109 (2). doi: 10.1007/BF00231783.

McIntyre CC, Mori S, Sherman DL, Thakor NV, Vitek JL, 2004 Electric field and stimulating influence generated by deep brain stimulation of the subthalamic nucleus. Clin Neurophysiol 115 (3), 589–595. doi: 10.1016/j.clinph.2003.10.033. [PubMed: 15036055]

Min H−K, Hwang S−C, Marsh MP, et al., 2012 Deep brain stimulation induces BOLD activation in motor and non-motor networks: an fMRI comparison study of STN and EN/GPi DBS in large animals. Neuroimage 63 (3), 1408–1420. doi: 10.1016/j.neuroimage.2012.08.006. [PubMed: 22967832]

Moeller J, Strother S, Siditis J, Rottenberg D, 1987 The scaled subprofile model: a statistical approach to the analysis of functional patterns in positron emission tomographic data. J Cereb Blood Flow Metab 7, 649–658. [PubMed: 3498733]

Moffitt MA, McIntyre CC, 2005 Model-based analysis of cortical recording with silicon microelectrodes. Clinical Neurophysiology 116 (9), 2240–2250. doi: 10.1016/j.clinph.2005.05.018. [PubMed: 16055377]

Paek SB, Min H−K, Kim I, et al., 2015a Frequency-dependent functional neuromodulatory effects on the motor network by ventral lateral thalamic deep brain stimulation in swine. Neuroimage 105, 181–188. doi: 10.1016/j.neuroimage.2014.09.064. [PubMed: 25451479]

Paek SB, Min H−K, Kim I, et al., 2015b Frequency-dependent functional neuromodulatory effects on the motor network by ventral lateral thalamic deep brain stimulation in swine. Neuroimage 105, 181–188. doi: 10.1016/j.neuroimage.2014.09.064. [PubMed: 25451479]

Papavassiliou E, Rau G, Heath S, et al., 2004 Thalamic Deep Brain Stimulation for Essential Tremor: relation of Lead Location to Outcome. Neurosurgery 54 (5), 1120–1130. doi: 10.1227/01.NEU.0000119329.66931.9E. [PubMed: 15113466]

Peña E, Zhang S, Deyo S, Xiao Y, Johnson MD, 2017 Particle swarm optimization for programming deep brain stimulation arrays. J Neural Eng 14 (1), 016014. doi: 10.1088/1741-2552/aa52d1. [PubMed: 28068291]

Peña E, Zhang S, Patriat R, et al., 2018 Multi-objective particle swarm optimization for postoperative deep brain stimulation targeting of subthalamic nucleus pathways. J Neural Eng 15 (6), 066020. doi: 10.1088/1741-2552/aae12f. [PubMed: 30211697]

Pollo C, Kaelin-Lang A, Oertel MF, et al., 2014 Directional deep brain stimulation: an intraoperative double-blind pilot study. Brain : a journal of neurology 137 (Pt 7), 2015–2026. doi: 10.1093/brain/awu102. [PubMed: 24844728]

Pouratian N, Reames DL, Frysinger R, Elias WJ, 2011 Comprehensive analysis of risk factors for seizures after deep brain stimulation surgery. Clinical article. J. Neurosurg 115 (2), 310–315. doi: 10.3171/2011.4.JNS102075. [PubMed: 21548744]

Rebelo P, Green AL, Aziz TZ, et al., 2018 Thalamic Directional Deep Brain Stimulation for tremor: spend less, get more. Brain Stimul 11 (3), 600–606. doi: 10.1016/j.brs.2017.12.015. [PubMed: 29373260]

Reker P, Dembek TA, Becker J, Visser-Vandewalle V, Timmermann L, 2016 Directional deep brain stimulation: a case of avoiding dysarthria with bipolar directional current steering. Parkinsonism Relat. Disord 31, 156–158. doi: 10.1016/j.parkreldis.2016.08.007. [PubMed: 27591075]

Richardson RM, Ostrem JL, Starr PA, 2009 Surgical Repositioning of Misplaced Subthalamic Electrodes in Parkinson’s Disease: location of Effective and Ineffective Leads. Stereotact Funct Neurosurg 87 (5), 297–303. doi: 10.1159/000230692. [PubMed: 19641340]

Ross EK, Kim JP, Settell ML, et al., 2016 Fornix deep brain stimulation circuit effect is dependent on major excitatory transmission via the nucleus accumbens. Neuroimage 128, 138–148. doi: 10.1016/j.neuroimage.2015.12.056. [PubMed: 26780572]

Saikali S, Meurice P, Sauleau P, et al., 2010 A three-dimensional digital segmented and deformable brain atlas of the domestic pig. J. Neurosci. Methods 192 (1), 102–109. doi: 10.1016/j.jneumeth.2010.07.041. [PubMed: 20692291]

Sandvik U, Hariz G−M, Blomstedt P, 2012 Quality of life following DBS in the caudal zona incerta in patients with essential tremor. Acta Neurochir (Wien) 154 (3), 495–499. doi: 10.1007/s00701-011-1230-z. [PubMed: 22109693]

Schmidt C, van Rienen U, 2012 Modeling the Field Distribution in Deep Brain Stimulation: the Influence of Anisotropy of Brain Tissue. IEEE Transactions on Biomedical Engineering 59 (6), 1583–1592. doi: 10.1109/TBME.2012.2189885. [PubMed: 22410323]

Slopsema JP, Cass R, Hjelle M, Johnson MD, 2019 Advancing Directional Deep Brain Stimulation Array Technology. In: Proceedings of the 2019 Design of Medical Devices Conference 2019 Design of Medical Devices Conference Published online April.

Slopsema JP, Peña E, Patriat R, et al., 2018 Clinical deep brain stimulation strategies for orientation-selective pathway activation. J Neural Eng 15 (5), 056029. doi: 10.1088/1741-2552/aad978. [PubMed: 30095084]

Springer, 2011 Molecular and Functional Models in Neuropsychiatry. Accessed September 10, 2019 http://public.eblib.com/choice/publicfullrecord.aspx?p=763654.

Steigerwald F, Müller L, Johannes S, Matthies C, Volkmann J, 2016 Directional deep brain stimulation of the subthalamic nucleus: a pilot study using a novel neurostimulation device. Movement Disorders 31 (8), 1240–1243. doi: 10.1002/mds.26669. [PubMed: 27241197]

Teplitzky BA, Zitella LM, Xiao Y, Johnson MD, 2016 Model-Based Comparison of Deep Brain Stimulation Array Functionality with Varying Number of Radial Electrodes and Machine Learning Feature Sets. Front Comput Neurosci 58. doi: 10.3389/fncom.2016.00058, Published online.

Tracey DJ, Asanuma C, Jones EG, Porter R, 1980 Thalamic relay to motor cortex: afferent pathways from brain stem, cerebellum, and spinal cord in monkeys. J. Neurophysiol 44 (3), 532–554. [PubMed: 7441314]

Vedam-Mai V, Krock N, Ullman M, et al., 2011 The national DBS brain tissue network pilot study: need for more tissue and more standardization. Cell Tissue Bank 12 (3), 219–231. doi: 10.1007/s10561-010-9189-1. [PubMed: 20589432]

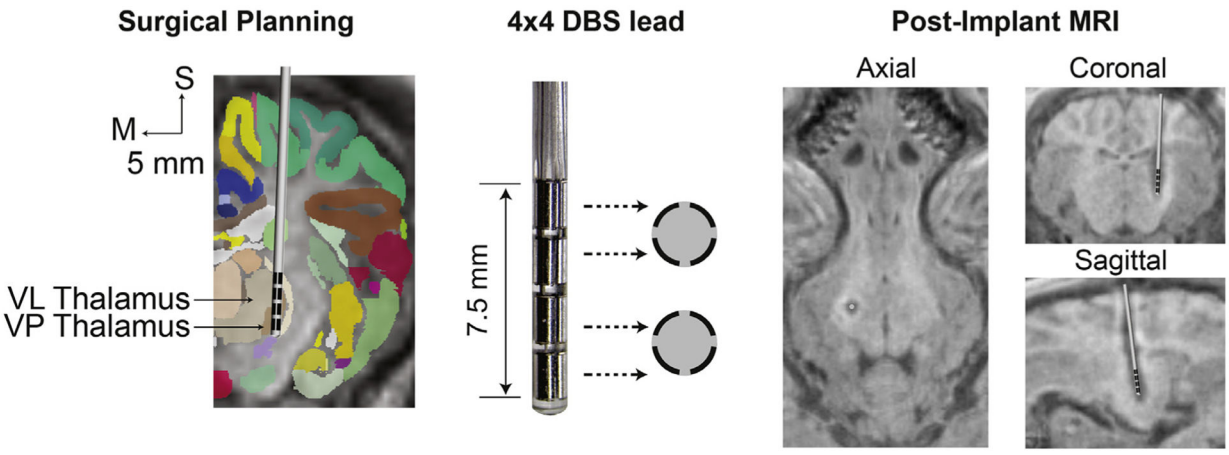

Fig. 1.

Experimental setup. A swine atlas was registered to a pre-operative MRI (a) to determine the location of the VL thalamus, a 16 channel (4 rows × 4 columns) DBS lead (b) was stereotactically implanted in the VL thalamus followed by postoperative anatomical MRI (c).

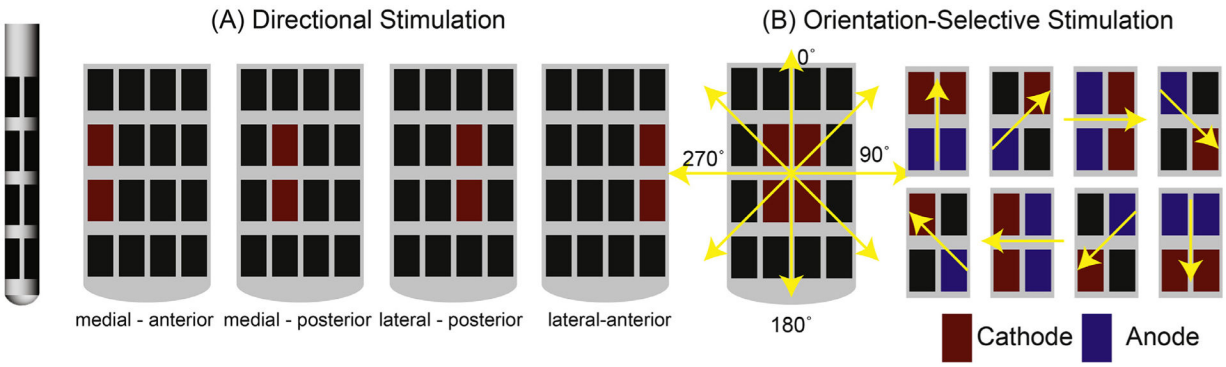

Fig. 2.

Stimulation was applied in two paradigms through a 16-contact directional DBS lead. (A) Unwrapped version of the lead showing directional stimulation where a pair of cathodes in each column were used to stimulate in each of the 4 directions around the lead. (B) Orientation-selective stimulation consisted of rotating a dipole 360° around a quad of electrodes.

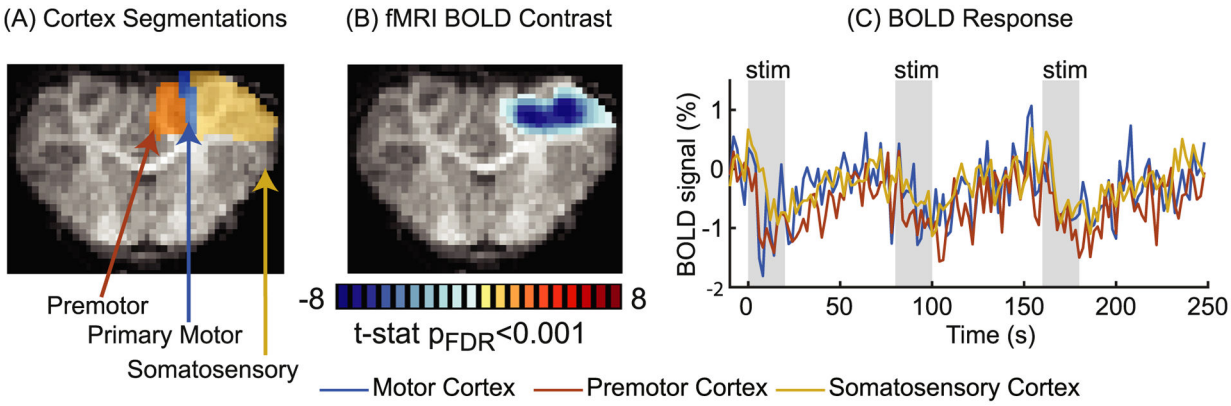

Fig. 3.

fMRI BOLD contrast in the sensorimotor cortex to VL-thalamus DBS. (A) Atlas-based segmentations of the somatosensory, premotor, and primary motor cortices. (B) An example of the BOLD contrast to VL-thalamus stimulation from a single trial. (C) An example mean time series of the response shown in (B). DBS was applied for 20 s followed by 60 s of no stimulation, repeated 3 times.

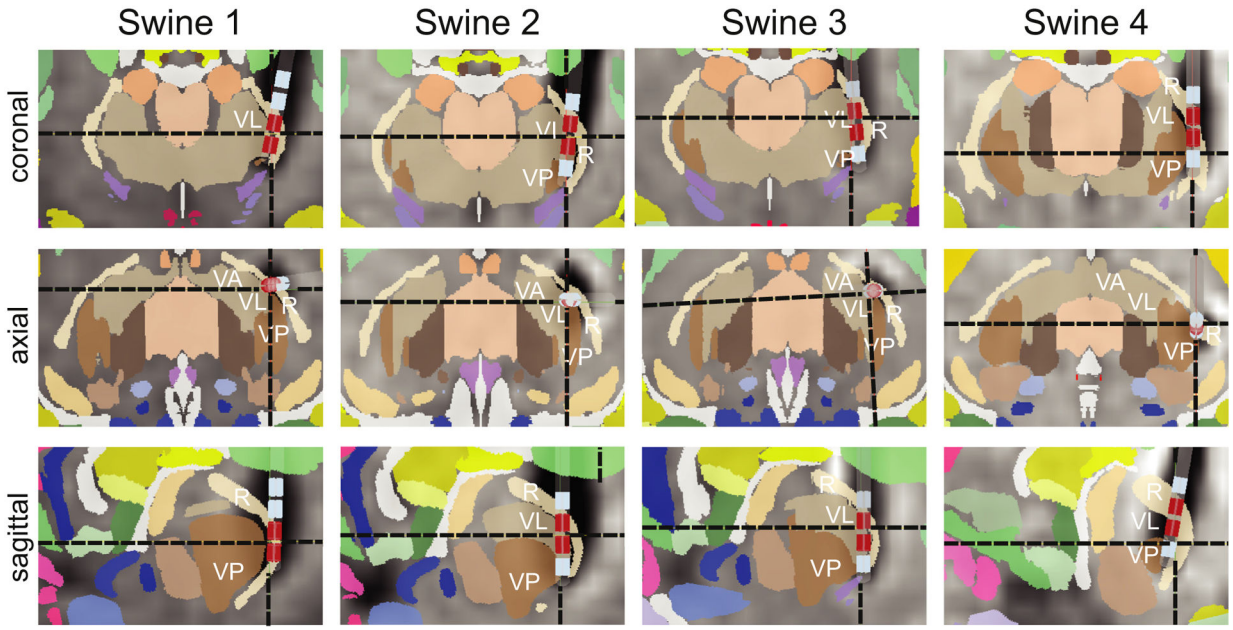

Fig. 4.

Localization of 16-contact DBS lead implants to the VL thalamus. (VL = ventral lateral, VA = ventral anterior, VP = ventral posterior, *R* = reticular). Anatomical post-implant UTE scan showing the artifact of the DBS lead is overlaid with a swine atlas. (Félix et al., 1999; Saikali et al., 2010).

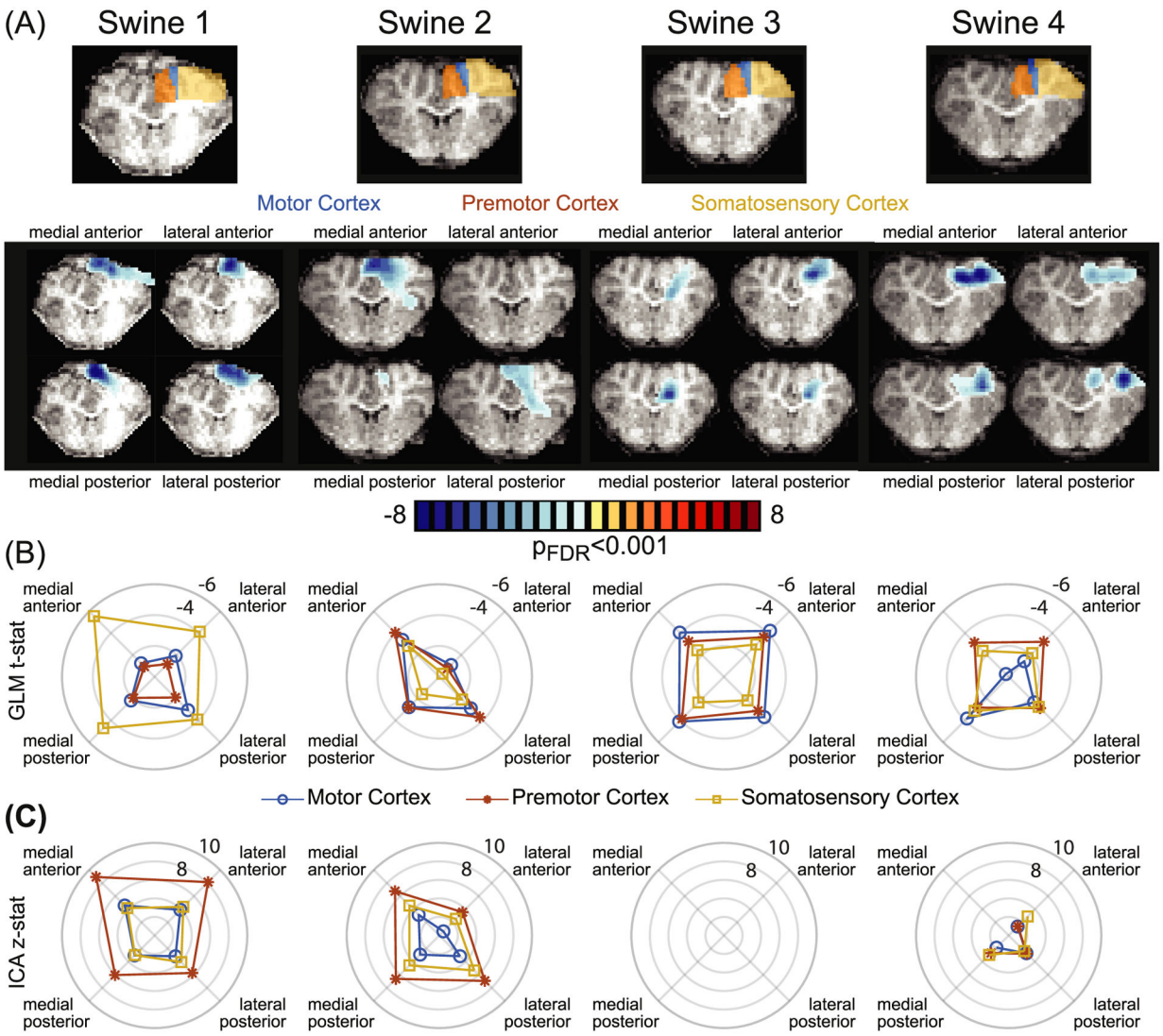

Fig. 5.

fMRI negative BOLD contrast is shown in the motor, premotor, and somatosensory cortices (A) when stimulating in four radial directions around the DBS lead. The negative BOLD contrast was quantified by the average t-statistic in the primary motor (blue), premotor (orange), and somatosensory (yellow) cortices using the GLM method (B) and the ICA method (C).

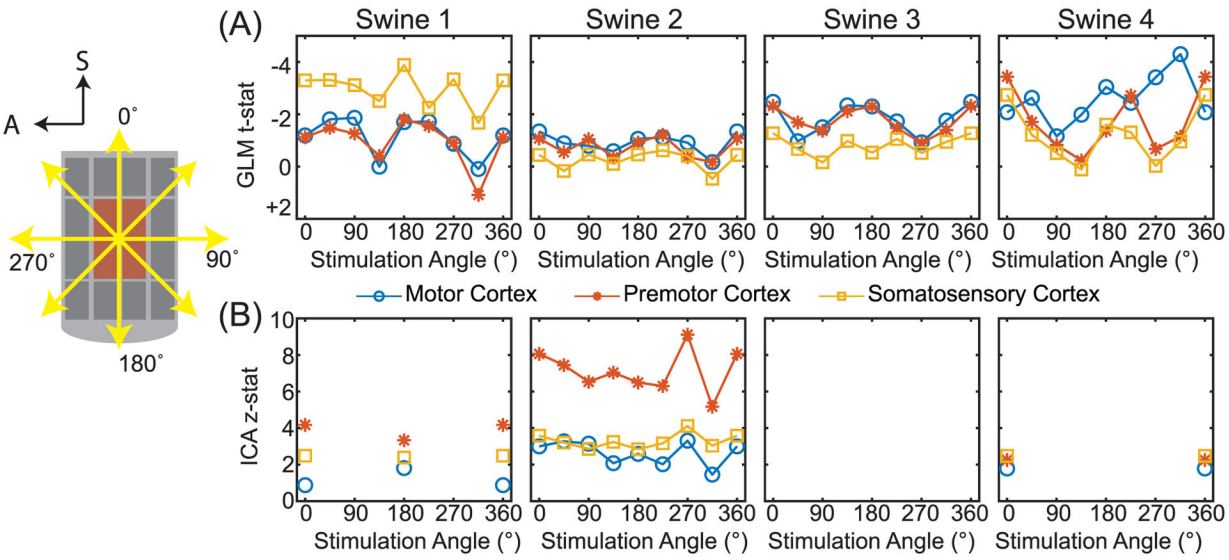

Fig. 6.

fMRI BOLD contrast during orientation-selective stimulation through a quad of electrodes on the medial side of the lead. 0°/180° represents orientation of the electric field parallel to the lead and 90°/270° represents orientation of the electric field perpendicular to the lead. The average t-statistic of significant voxels within each cortical region was quantified for each orientation using the GLM method (A) and the z-statistic using the ICA method (B).